Construction and Building Materials 271 (2021) 121569

Contents lists available at ScienceDirect

Construction and Building Materials

journal homepage: www.elsevier.com/locate/conbuildmat

Sample key features affecting mechanical, acoustic and thermal properties of a natural-stabilised earthen material

Carlos Rivera-Gómez *, Carmen Galán-Marín, Victoria P. López-Cabeza, Eduardo Diz-Mellado

Departamento de Construcciones Arquitectónicas 1, Escuela Técnica Superior de Arquitectura, Universidad de Sevilla, Avda. Reina Mercedes, 2, Seville 41012, Spain

HIGHLIGHTS

- A comprehensive analysis of the interaction of different properties is proposed.
- Acoustic and thermal performances are related to porosity.
- Transmission loss is affected by the use of reinforcement fibers.
- Soil selection is a key factor in determining stabilized earth materials performance.

ARTICLE INFO

Article history:
Received 2 June 2020
Received in revised form 20 September 2020
Accepted 30 October 2020
Available online 19 November 2020

Keywords:
Vernacular architecture techniques
Earthen materials
Thermal conductivity
Noise mitigation
Biocomposites
Fiber-reinforced soil
Green buildings

ABSTRACT

The use of natural materials has become more important as a result of the growing need to conserve energy, exploit renewable materials, and incorporate architecture and construction into sustainable methods of production. Accordingly, the present work investigates the engineering properties of a new earthen building material. This proposal is based on traditional unfired earthen masonry and consists of compressed earth blocks stabilised with natural polymers and wool fibers for use as insulating and structural load-bearing walls in buildings. The conducted experimental study enabled us to determine the mechanical performance, thermal conductivity, noise mitigation, modulus of elasticity, porosity percentage, and diameter through mercury intrusion porosimetry. The influence of soil characteristics on thermophysical and acoustic properties of tested material were investigated. The experimental data show good efficiency and a significant improvement in the engineering properties of these materials compared to traditional compressed earth blocks. In this research, a comprehensive analysis of the interaction of different properties is proposed as an assessment methodology that could be applied to any kind of stabilised soil material. The correlation of the results, being the type of soil the only variable of the analyzed samples, has allowed identifying sample key features and tests so as to obtain the best mechanical, thermal and acoustic performances.

1. Introduction

In the current situation in which the model of human growth is increasingly revealed as an unsustainable path, since it involves a growing demand for finite raw materials, greater energy consumption and an increase in greenhouse gas emissions [1-4], it is of utmost importance to revisit eco-friendlier traditional construction methods, adapting them from new technological standpoints.

Despite the downturn following the economic crisis of 2008, the construction industry continues to be one of the main and most active sectors throughout Europe, directly and indirectly representing about 28% of employment in industry and an average of 7.5% of the European economy in terms of GDP [5]. With an annual turnover of 1200 billion euros, this sector accounts for 25% of all European industrial production, reaching, in the case of Spain, more than 124 billion euros considering civil engineering works, residential buildings, and refurbishment interventions [6]. Current forecasts seem to indicate that, in global terms, the construction industry will continue to grow at a rapid pace over the next decade.

Although from a contemporary perspective, it could be seen as a building material of the past, almost 50% of the world's population lives nowadays in earth-based housing [7]. While it is true that most of earth constructions are located in developing countries, it is also true that this type of construction can be found in developed countries as well, such as in Europe, the United States, Brazil, or Australia [8,9]. Raw earth is, in fact, the subject of renewed interest in developed countries, although these new initiatives face

* Corresponding author.
E-mail address: crivera@us.es (C. Rivera-Gómez).

https://doi.org/10.1016/j.conbuildmat.2020.121569
0950-0618/

in some of these countries many problems, including the absence of regulations. Guidelines about earth materials are quite uneven depending on the country, which determines the difficulties for the constructive use of these types of materials despite their environmental advantages and their growing demand. Several countries already have earth construction-related standards. In Spain, since 2008 with the standard UNE 41410:2008 [10] publication, the country occupies a leadership position in the field of European earth regulations, as this standard is the only non-experimental regulation in Europe. In 2008 the German Foundation for the Environment proposed a set of technical recommendations known as the "Lehmbau Regeln" [11]. In 2001 the Australian Earth Building Handbook [12] was published. In New Zealand, the earth building regulations are set according to the maximum height of the building [13]. And, in the Southern African community, since 2014, a regulation based on the "Code of Practice for Rammed Earth Structures" [14] is available. Most of these standards refer to structural considerations, leaving aside others relating to performance aspects such as thermal conductivity and noise mitigation, which would favor the systematisation of recommendations for the constructive use of this type of earth-based materials.

The physical properties of different formulations of earth materials have been studied on their own, or by comparison with other building materials. In most cases by addressing their mechanical performance [15-17]. The analysis of thermal performance of earth-based materials has been also widely studied in the literature [18-27]. Recently, Narayanaswamy et al. [18] concluded that thermal conductivities of these materials using the processed ground blast furnace slag were noticeably lower. Saidi et al. [28] obtained some results showing that the thermal conductivity of stabilised earth bricks increases as a function of stabilisers contents. And Rincón et al. [29] investigate the microclimatic potential of earth walls due to their high thermal inertia. Far less work has been done to quantify the noise mitigation and sound frequency response of these materials [30-33]. Ben Mansour et al. [34] proved that the acoustic and mechanical behavior of CEBs were strongly influenced by the applied compaction pressure including, inter alia, the bulk density of the specimen and the added cement used as stabilizer. Tamas-Gavrea and Dénes [35] determined in their work the high acoustic absorption at high frequencies (0.93 at 2360 Hz) of an earth mortar with rice paste and sheep wool fibres. Finally, Niresh et al. [36] studied the sound absorption characteristics of the single and multi-layered porous materials with the help of an impedance tube. Earthen materials reveal a great disparity in the results of these insulation properties. This is due to the significant differences between the manufacturing and stabilization methods but, principally, in the composition of the soils used to produce them [37]. Hence the importance of evaluating the influence of soil parameters in physical–mechanical characteristics of earthen materials, such as mechanical resistance, thermal conductivity, and also their acoustic properties, due to the scarcity of studies in that regard [38]. The influence of the formulation of the soils and namely the chemical and mineralogical composition, the plasticity index, and the resultant porosity in the mixes, are also considered important towards the evaluation of the behavior of each sample and the improvement of its characteristics towards optimisation. Considering that indoor comfort mainly depends on temperature, humidity, and noise abatement [38], not only mechanical but thermal and acoustic comfort, are particularly significant factors towards achieving optimal building habitability.

The present research involves three different types of clayish soil, in terms of chemical composition, texture, and appearance used to produce natural polymer-stabilized earth blocks. The mixes are based on soil, wool fibers, and alginate, a natural polymer obtained from seaweed. The mixes were prepared under controlled laboratory conditions where the samples were produced and then characterized in dry state. Several tests were performed on the samples to evaluate the physical–mechanical properties such as thermal insulation, thermal conductivity, noise mitigation, modulus of elasticity, determination of the porosity distribution through mercury intrusion porosimetry, and mechanical performance. Additionally, the microstructure of the samples was studied by Scanning Electron Microscopy (SEM) in order to better determine pore size and internal microcracks features.

The aim of this paper is the evaluation of the mechanical, thermal, and acoustic properties of three soil formulations of a new eco-efficient clayish earth material. Since the only mix variable is the type of soil, the study aims to define an assessment methodology by identifying which are the most decisive soil test results, and which physical characteristics of the samples, after the curing process and for this type of natural-stabilised earthen materials, most affect the final efficiency of the analysed building products in order to determine those with the best overall performance.

2. Materials and methods

2.1. Raw materials

The three types of soil used in this study were provided by the Andalusian Technological Center of Ceramics (INNOVARCILLA) [39]. Clayish soils were collected from the area of Bailen (Spain), all of them being common raw materials in the manufacture of ceramic products in the local industry. Due to their appearance, the soils are named after their colour: red, yellow, and black. Once in the laboratory, soils were dried and crushed with a ball mill so as to obtain a powder between 1 mm and 200 μm. Their mineralogical composition and Atterberg limits classification were determined and carried out by X-ray diffraction with an X-ray powder diffractometer, XRD, (Empyrean PANALYTICAL) and according to ASTM D 422 [40] and ASTM D 4318 [41] respectively. The results are shown in Table 1. Similarly, untreated animal wool was used as a reinforcement fiber. Sheep wool was obtained from Spanish agricultural surpluses that turn hundreds of kilos of this material into agroforestry waste every year. The fibers were unraveled from raw sheep fur and cut to 10 mm in length before being added to the mixes.

2.2. Stabilization and sample preparation

The stabilizer used was alginate, specifically a formulation called CIMALGIN HS4 manufactured by the company CIMAPREM [42] consisting of a white-greyish powder. The use of this variety was due to the length of the gelling process that allowed the samples to be completely shaped by its components. The alginate is a natural polymer that contributes not only to flexibility and strength but also has a high water-retaining capacity, improves viscosity, stabilizes emulsion s, and provides cohesion to mineral particles and soils [43]. Previous research has corroborated the benefits of the use of wool fiber and alginate as earthen materials stabilizers [44]. To produce of the samples from the three soil types: red, yellow, and black, the same dosage was used as it is displayed in Table 2. The percentage of stabilizer used was decided based on previous research results [44].

The products tested consisted of CSEB (compressed stabilized earth blocks) as all samples were pressed and stabilized. For the performance of the scheduled tests, specimens of different sizes were produced. For this purpose, two laboratory presses were used: a manual block press manufactured by the company GRACOMAQ and a hydraulic press model MIGNON SS and branded NANNETTI. The number and size of the samples are reported in Table 3. The lab codes assigned to the samples were SR for red soil, SY for

Table 1
Chemical composition and physical characteristics of the three soils.

Soil sample			Red	Yellow	Black
Chemical analysis (bulk) (%) in weight	SiO_2		58.5	56.6	54.2
	Al_2O_3		16.7	12.1	12.3
	Fe_2O_3		7.0	4.2	4.3
	MnO		0.1	0.0	0.1
	MgO		2.8	2.2	2.1
	CaO		2.2	9.1	10.4
	Na_2O		0.2	1.7	1.4
	K_2O		5.0	3.1	2.9
	TiO_2		0.8	0.0	0.7
	P_2O_5		0.2	0.0	0.1
	L.O.I.		0.08	10.8	12.2
Mineralogical composition	Clay minerals (%)	Q	32	40	43
		Fd	5	tr.	3
		C	tr.	15	18
		D	10	tr.	4
		Fl	53	45	32
	Phyllosilicates (<2 μm) (%)	Sm	Ud.	40	32
		Ill	66	60	58
		Ka	33	Ud.	10
		Ch	tr.	tr.	Ud.
		P	Ud.	Ud.	Ud.
Grain-size distribution	Rejection at 63 μm(obtained by wet sieving) (%)		51.1	23.8	43.8
Atterberg limits	Liquid limit (%)		25.6	32.8	38.8
	Plastic limit (%)		14.1	11.1	18.6
	Plasticity index (%)		11.5	21.7	20.2

Table 2
Percentages of the different components of the samples.

Sample components	Quantity (gr)	%
Soil (red, yellow or black)	3070	76,75
Alginate	120	3,00
Water	800	20,00
Organic fiber (Sheep wool)	10	0,25

Table 3
Number and sizes of the manufactured samples according to the test.

Test	Number of samples per sample composition (SR, SY, and SB)	Dimensions of each sample (mm)
Dry bulk density	4	160 × 40 × 40
Thermal conductivity	3	108 × 54 × 12
Acoustic characterization	5	108 × 54 × 12
Modulus of elasticity	5	160 × 40 × 20
Mechanical testing (Compression strength)	6	40 × 40 × 40
Mechanical testing (Flexural strength)	6	160 × 40 × 40
Hg porosimetry	1	78 × 40 × 40
Calorific value	1	78 × 40 × 40

yellow, and SB for black soil respectively. All the samples were covered with plastic film and kept at room temperature for a curing during 28 days before being tested.

2.3. Physical and mechanical testing

2.3.1. Dry bulk density

The dry bulk density of each sample was determined following the UNE EN 772-13:2001 standard [45] for densities greater than 1,000 kg/m^3. To carry out the tests, a precision balance branded METTLER, model TOLEDO, with an accuracy of 0.01 g, was used. According to this procedure, samples are first dried in an oven at a (60 ± 3)°C, in order not to alter the organic nature of each sample. The constant mass is reached when the mass loss does not exceed 0.2% of the mass of the piece, between two consecutive weighing processes performed at 24-hour intervals. The final dry mass (m_{dry}) is registered. The apparent volume corresponds to the sample volume plus closed-pore volume being obtained from its length, width, and height, through a digital caliper, following the mathematical expression:

$$V = l_u \times w_u \times h_u (mm^3) \quad [1]$$

To calculate the dry bulk density of each sample, the final dry mass (m_{dry}) is divided by the apparent volume (V_g) of each piece according to the equation:

$$\rho_p = \frac{m_{dry}}{V_g} \times 10^6 \left(\frac{kg}{m^3}\right) \quad [2]$$

2.3.2. Thermal conductivity testing

The determination of thermal conductivity is based on an adaptation of the hot wire technique performed by the commercial equipment THB (Transient Hot Bridge), model THB-1, branded LINSEIS, with an accuracy of 0,00001 W/mK. The hot wire technique, established in standards like the UNE-EN ISO 8894–1:2010 [46] and UNE-EN 993-15:2005 [47], is a non-stationary measuring method (dependent on measurement period) whose greatest advantage is a significant reduction in comparison to the time required in stationary measuring methods. Previous to the performance of the test, a calibration of the equipment is carried out using a PMMA standard [48] measured with the aid of a pattern. To this end, the sensor is placed between the two PMMA test pieces, without projecting out the sides, making a sandwich, the readings of its thermal conductivity are then registered, and the obtained value validated, calibration of the equipment is thus completed (Fig. 1).

After calibration of the equipment, five rectangular test pieces of 108 × 54 × 12 mm were taken from each one of the samples whose thermal conductivity is intended to be determined, with at least one of the faces forming a rough plane. Test pieces are dried in an oven at (60 ± 3)°C, as not to alter the organic nature

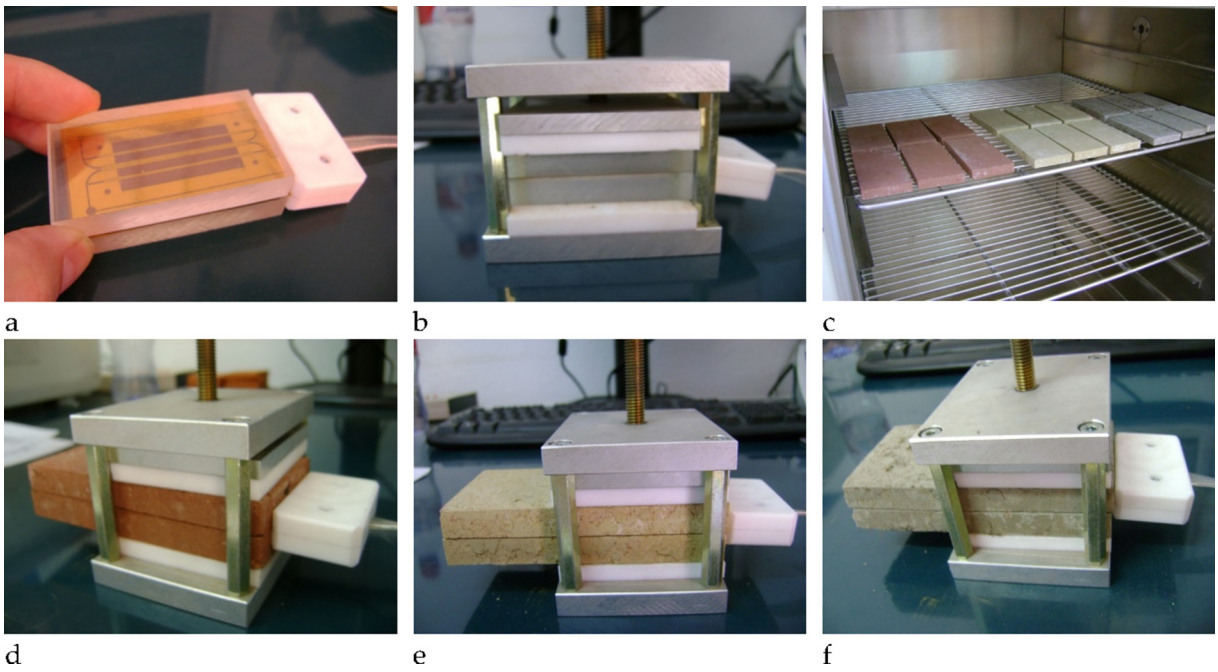

Fig. 1. a), b) and c) Equipment calibration and sample preparation. d), e) and f) thermal conductivity tests performed on the SR, SY, and SB samples respectively.

being subsequently left in a monitored desiccator at room temperature to cool down, avoiding any surface dust before measuring the thermal conductivity. For determination of the thermal conductivity, a sensor is positioned between both sample layers, ensuring proper contact between its surface and the surface of the sensor. An electric current is then applied to the sensor; generating a heat flow which gives rise to an increase in temperature. This thermal upsurge corresponds to the properties of the heat transport of the material and, therefore, allows the determination of its thermal conductivity.

2.3.3. Acoustic characterization

To perform the test, cylindrical samples were prepared using a BCN3D IGNIS laser cutter with an optical system and X-Y axes. The optical system formed by the laser tube, the mirror, and the lens, was used to focus the radiation beam from the laser tube, through the mirrors to the 4″ focal-length lens located at the head of the device. The laser beam was moved over the work surface by the action of the motors of trails X, Y. The following figure shows a diagram of the equipment (Fig. 2).

Average sound frequency response and transmission loss measurements were determined by means of a impedance tube branded BRÜEL&KJAER model 4206-T, with an accuracy of 1 Hz. The components of the acoustic testing setup consisted in two 29 mm diameter impedance tubes (50 Hz – 6,6kHz), a power amplifier model 2735, with two user-selectable gain settings of 0 dB and 20 dB, a sound calibrator model 2431 with an accuracy of ± 0.2 dB, four (¼ inch) pressure-field microphones model 4954-B, with a sensitivity of 2.8 mV/Pa, PULSE™ analysis software [49] and a laptop (Fig. 3). Tests were performed in accordance with the international standards: ASTM 1050-12 [50] for absorption coefficient, and ASTM E2611-17 [51] for transmission loss. The reverberation room method is superior to the impedance tube method regarding transmission loss testing in some respects. First, the measurement is performed with a diffuse sound field, i.e. under conditions which are closer to many practical installations. Second, there are no limitations concerning the type and construction of the absorber. Nevertheless, with the impedance tube can be obtained the normal incidence absorption coefficient of a sample with a small diameter (usually less than 10 cm). The results can be used to compare the basic absorption performance of a material and for acoustics simulations. This method has previously been used to determine the sound attenuation values of different porous materials [52-54]. Cylindrical samples, 29 mm in diameter, were tested, once mechanized as described before, within the frequency range between 500 and 6400Hzaccording with the standards procedures. The dynamic range of the analyzer greater than 85 dB, and the signal-to-noise ratio greater than 10 dB.

The test device must be calibrated before performing acoustic measurements. This is done by performing two signal measurements received by both microphones, interchanging their positions. Once the calibration is performed, the microphones were placed back in their original positions and the measurement of each sample is performed. The signal generated by each speaker is a plane wave and the power was approximately 100 dB since a signal of at least 10 dB above the background noise must be generated. Before placing each of the test samples in the sample holders, its thickness was measured, with an accuracy of 0.01 mm. Secondly, the sample was placed inside the sample holder tube. Then, due to the dimensions of the test samples and to ensure their water-tightness, they were sealed on the lateral sides with vaseline (petroleum jelly) so as to avoid mistakes caused by the loss of an acoustic signal in the case that the sample is not properly sealed with the impedance tube. Finally, the O-ring (sealing ring) is positioned and the sample holder is screwed on (Fig. 4).

Acoustic measurements were determined as the difference between the level of the incident and the transmitted acoustic power, in other words, the drop in the level of acoustic power of a wave when going through the filter. Transmission Loss (TL) calculation is obtained according to the equation:

$$TL = 10 \cdot log \frac{W_i}{W_t} = Lw_i - Lw_t \quad [3]$$

where (W_i) corresponds to the incident) power, (W_t) the transmitted power, and (Lw_i) and (Lw_t) refer to the incident and transmitted acoustic pressures, respectively.

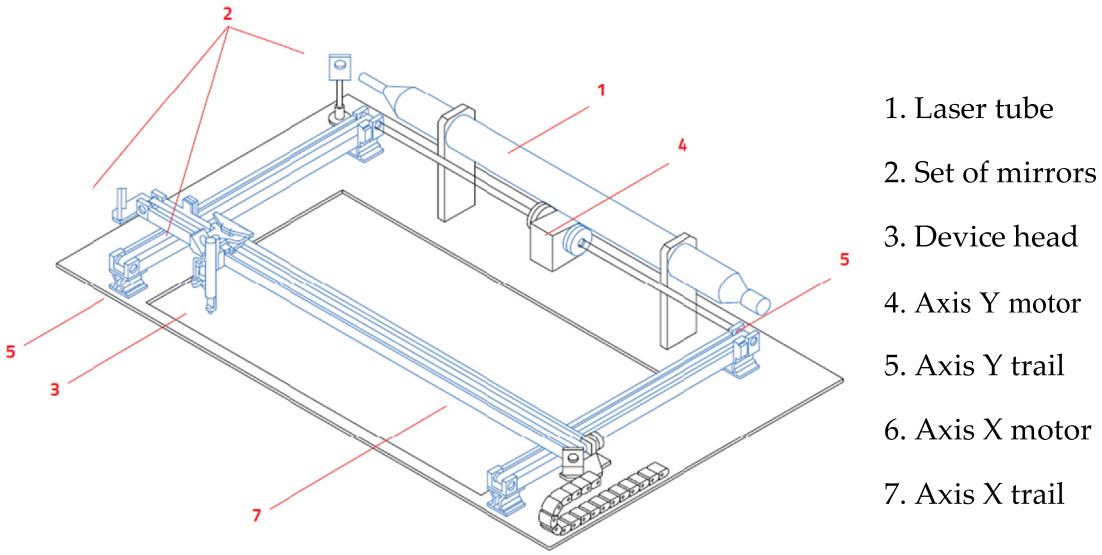

Fig. 2. Components of BCN3D IGNIS laser cutter, used for the preparation of the samples.

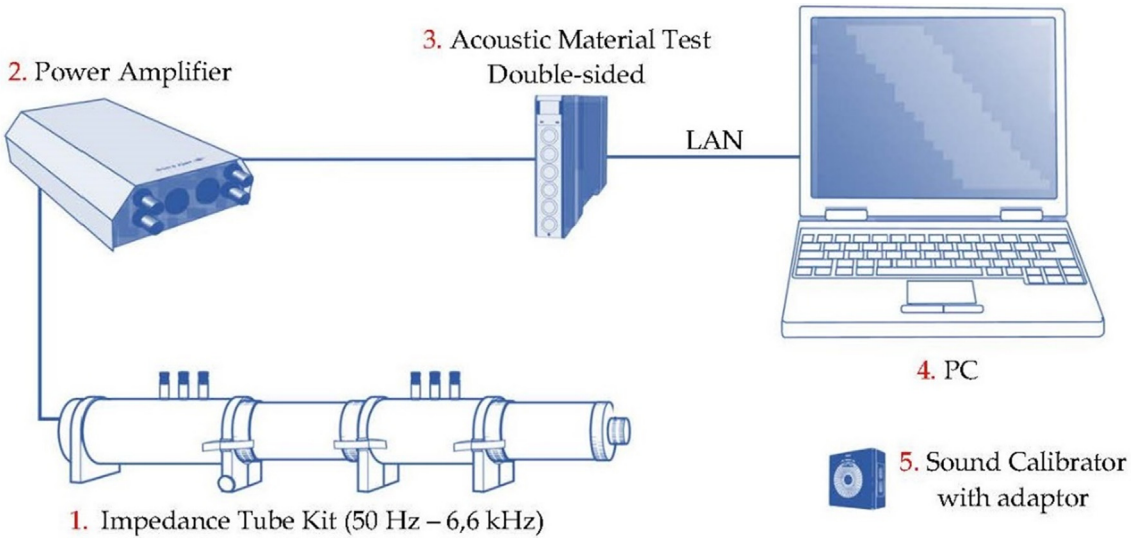

Fig. 3. Experiment setup used to perform the acoustic tests.

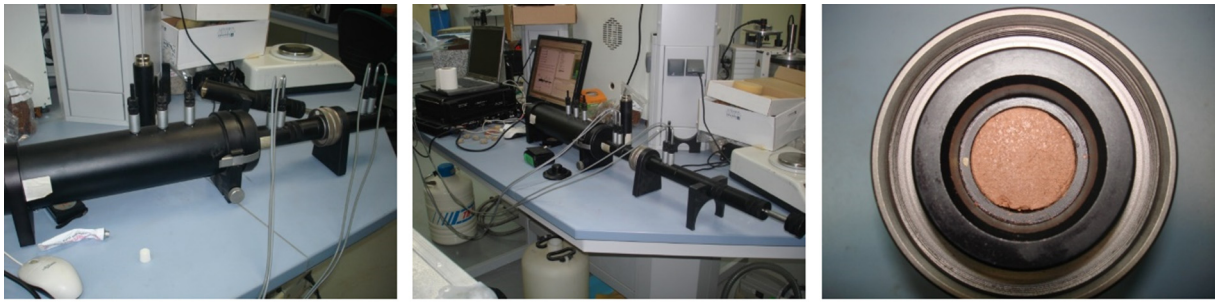

Fig. 4. a) and b) Test setup with the impedance tube kit. c) Test sample placed inside the tube.

2.3.4. Dynamic modulus of elasticity measurement

The dynamic modulus of elasticity, or dynamic Young's modulus (MOE), is an intrinsic material property, which can be determined through ASTM E1875–13 standard [55]. Following this standard, in the present research, MOE was determined from the resonant frequency of the material in response to an impact. With the purpose of performing the tests, a data acquisition module branded BRÜEL & KJAER, model 3052, with an accuracy of

0.1 kHz, a piezoelectric accelerometer (of up to 6000 Hz) branded BRÜEL & KJAER, model 4500-A, with a sensitivity given in the calibration of 0,316 pC/ms^{-2}, and a modal hammer sledge branded BRÜEL & KJAER, model 8208, sensitivity of 0.225 mV/N, were used.

For each of the mixes, a minimum of 4 samples, with the appropriate dimensions to guarantee a resonant frequency lower than 6000 Hz, were obtained by using a disc cutter. Once prepared, the samples were dried in an oven at (60 ± 3) ºC, so that their organic nature does not result altered. Afterward, the samples were cooled in a desiccator, in the room where the measurement is performed including the sensor in it, to favor the tempering.

The samples were placed on the flexing support system, the distance between each support and the corresponding end of the test piece was 0.224 L, being L the length of the sample. The accelerometer was placed on the sample surface, coinciding with one of the supports. The impacts were applied on the center of the sample. Samples preparation and their arrangement on the flexing support system during the test are shown in Fig. 5.

MOE determination test was performed by impulse excitation of vibration and the subsequent analysis of the resonant basic frequency. The most important task is to obtain the fundamental mode resonant frequency when the specimen is subjected to an instantaneous pulse (beating) and to register the signal or the frequency spectrum that this beating produces. The signal is analyzed by Fast Fourier Transform (FFT) with adequate software. From the value of the corresponding resonant frequency, (f) given in Hz, of the first harmonic's wavelength, 2L in m, can be obtained the pulse velocity (v) in m/s.

$$v = 2Lf \tag{4}$$

being (L) is sample's length (0.160 m).

And, using the density value, (ρ) en kg/m^3, it is possible to calculate the MOE value:

$$MOE = \rho v^2 \tag{5}$$

The value used as resonant frequency is the average value of six successive readings obtained with a maximum difference of 1% between them.

Holding the specimens in the corresponding face to the bottom of the mould (face 1) and rotating them 90°and holding them in a lateral side of the mould (face 2), successive readings of the flexural resonant frequencies are made. Specifications described in ASTM E1875–13 standard [55] referring to the conditions of the holders, results calculations, etc., have been followed.

2.3.5. Mercury intrusion porosimetry determination

In the current work, the porosity characterization of the dry samples was performed through Mercury Intrusion Porosimetry (MIP), a technique through which the pores are infiltrated with mercury as a result of the application of pressure. This technique is based on the capillarity generated by the mercury, which does not dampen the solid it is in contact with. The mercury does not spontaneously penetrate the capillary pipes but requires a pressure inversely proportional to the diameter (D) of the pipes or pores through which it intrudes. [56]. This filling and controlled pressure cast generate intrusion and extrusion curves characteristic for each material, in the range of pore sizes, 0.003–360 μm. The MIP does not only turn out to be of enormous interest for covering a wide range of pore sizes (five orders of magnitude) but because the data that it provides (volume of intruded mercury intruded according to applied pressure) is indicative of different characteristics of the porous space and may correlate with different physical properties of the material [57]. The measurement was carried following standards: ASTM D 4284-03 [58] and ASTM D 4404-84 [59]. For non-wetting liquids like mercury, and cylindrical pores, this phenomenon is expressed by the Lucas–Washburn equation [60]:

$$D = -4g\cos q/P \tag{6}$$

where (P) corresponds to the applied pressure, (D) is the diameter of the pore, (q) the contact angle of between the solid and the mercury, and (g) refers to the surface tension of the fluid.

This method provides the volume of the sample (V_c) and the volume of the pores filled with mercury (V_{pores}) which enable determination of the effective porosity, open to the penetration of the mercury, ($E\%$) according to the expression:

$$E\% = (V_{pores}/V_c)x\,100 \tag{7}$$

The total porosity ($TP\,\%$), accesible and inaccesible, cannot be calculated using MIP. Densities of the sample are included in its calculation.

$$TP\% = 100\,x\,(1 - D_b/D_r) \tag{8}$$

where (D_b) is the bulk density, established as the relation between the dry mass and the volume of the test piece, and (D_r) corresponds to the skeletal density of the mineral or grain phase (specific weight), obtained through the helium pycnometer testing.

Different parameters concerning the samples analyzed in the current research were obtained through MIP: Total intrusion volume, Total area of pores, Average diameter of the pore (concerning the volume or area), Apparent density (of the sample fragment at a certain pressure, 0.00262 MPa), Skeletal density, Porosity ($E\%$) (defined as the relation between the total volume of pores (V_{pores}) and the total volume of the sample (V_c), and Percentage of the capillary.

MIP tests were performed using the model AUTOPORE Series IV 9500, branded MICROMETRICS with pore size ranges from 0.003 to 1100 μm, and an accuracy of 0,005 μm. The equipment allows, through the forced intrusion of mercury, the measurements of pore diameters in a range between 0.003 mm and 360 mm. Once samples were dried in an oven at 60 °C for 24 h and placed in the sample holder, two consecutive measurements, one at low pressure

a b c

Fig. 5. a) Mechanization of the 158 × 40 × 40 mm samples. b) Equipment for determining MOE by impact and c) MOE test performance.

and another one at high pressure until it reaches the limit imposed by the equipment and its consequent depressurization were required to perform the measurements. Pores with diameters between 360 mm and 3.6 μm are intruded in the range of low pressures (345 kPa), while in the high-pressure port, the maximum pressures are reached (228 MPa), and the range of pores studies varies from 6 mm and 0.0055 μm in diameter. The glass sample holders (penetrometers) have a conductively coated capillary that allows registration of the volume of mercury lodged in it through its capacitance, as well as its variation in the successive increases in pressure.

2.3.6. Mechanical assessment

Flexural strength tests procedure: Bending strength was determined on six specimens for each mix under study by using the three-point test on the specimens, in agreement with the specifications of UNE-EN 1015–11:2000/A1:2007 standard [61] for the determination of bending strength of mortars used for rough castings and mortar linings. Flexural tests were conducted at room temperature (20 °C) on a multi-test machine branded CODEIN S. L., model MCO-30/139, (maximum load 10 kN), with an accuracy of 0,2N, in a three-point bending configuration. These tests provided two mechanical properties for the analyzed samples, namely, the ultimate stress and the ultimate strain.

Compressive strength tests procedure: After breaking the prismatic specimen in a three-point bending strength test, each half was used to determine compressive strength. Tests were conducted following the same UNE-EN 1015-11:2000/A1:2007 standard [62]. A total of 36 compressive strength tests were conducted. The equipment used was the same CODEIN S.L., MCO-30/139 multi-test machine than was previously employed for the performance of the flexural tests.

2.3.7. Moisture and calorific value determination

The calorific value of the samples and the water content was also determined, both on a dry and wet basis. For a proper understanding of the subsequent results, the following definitions should be kept in mind:

The Higher Calorific Value (HCV) is defined as the total quantity of heat given off in the complete combustion of a volume unit of the material, when the water vapour caused by the combustion is condensed and, as a consequence, the heat given off in this phase change is measured.

Lower Calorific Value (LCV) or net calorific value, is the total quantity of heat given off in the complete combustion of a volume unit of the material without taking into account the fraction corresponding to the latent heat from water vapor generated in the combustion, considering no phase change, and it is expelled as vapor.

The methodology followed for the determination of the moisture of each sample is based on the following applicable standards: UNE-EN ISO 18134-1:2016 [48], UNE-EN ISO 18134-2:2016 [63], and UNE-EN ISO 18134-3:2016 [64]. Similarly, the methodology through which the determination of the calorific value of each of the three samples was performed is detailed in the UNE-EN 14918:2011 standard [65].

Samples preparation was performed through the prior grinding of a fraction of each material, using agate mortar. Quantification of water content is performed through oven drying to constant mass at a temperature of 60 ± 5 °C, to alter the composition of the samples. To measure the calorific value, due to the low density of the samples tested, it was necessary to prepare the bars for each one of the materials, through pressing of 0.5 ± 0.01 g of mass, a force strong enough for producing a compact test piece under the specifications of the calorimeter used to perform the test.

The calorimetric determination consisted of two separate experiments: the combustion of the calibration material (benzoic acid) and the combustion of each of the three samples analysed, all under the same conditions. The calorimetric procedure for the two types of experiments was essentially the same and consists of quantitatively carrying out a combustion reaction (with a high oxygen pressure in the calorimetric bomb) on defined combustion products, and of measuring the change in temperature caused by the whole process. The adiabatic calorimetric bomb used, or oxygen combustion calorimeter, was the model 6300, branded PARR, which is configured to ensure an accuracy of 0,1%.

2.3.8. SEM analysis

Additionally, in order to complement the results of the porosimetry study, Scanning Electron Microscopy (SEM) analysis was performed. SEM is a useful tool not only to verify the structure and topography of the samples but also to achieve the direct monitoring of polymer-soil and fiber-soil matrix interfaces [43]. Different SEM studies have been useful to illustrate the spatial correlations between the numerous components within soil matrices [32,66]. The samples, in this research, were examined using a JSM-6460LV model, branded JEOL, scanning electron microscope. Several samples of each soil-mix were analyzed at low and high magnification for identification of their morphological features, the variations in the pore distribution networks, and the internal drying microcracks features.

3. Results and discussion

In this section, the main results of the three mixes tested (SR, SY, and SB) will be displayed and confronted with the main objective of identifying the soil characteristics determining better thermal, acoustic and mechanical global performance.

3.1. Porosimetry of mercury intrusion (MIP)

In this work, the applicability of the mercury intrusion technique has been used to the study of the porosity and pore size distribution of samples of three natural-polymer stabilized soils. The analysis aims at a better knowledge of the structure of the samples, that is, their mechanical, thermal, and acoustic properties. In the following plotts, some of the results obtained for the porosity analysis of the three samples tested are shown (Figs. 6-7). A higher porosity 36,18%, and a lower average pore diameter 57,8 nm in SR can be appreciated, these results correspond to a more homogeneous distribution of the pores in the sample as observed in Fig. 6. By contrast, SY and SB have much higher average pore diameters 115,2 nm and 129,9 nm, respectively, for lower percentages of porosity, 35,85% for SY and 32,83% for SB. This indicates a worse distribution of pores in these samples. Furthermore, correlating porosity with the uncertainty of the dry bulk density, much higher for SB 1,390 (±130) kg/m^3, this indicates that, not only the pore distribution is more irregular in these samples, but also that these disparities imply a greater heterogeneity of the internal features among them.

3.2. Acoustic characterization

The acoustic characterization, determination of the sound frequency response of the samples of the three soil types stabilized with alginate and reinforced with wool fibres is represented graphically below (Fig. 8).

In the previous figure, the curves show that SY samples present a greater loss than the rest of the samples, approximately 2 dB higher than SR samples and 4 dB in comparison with the SB sam-

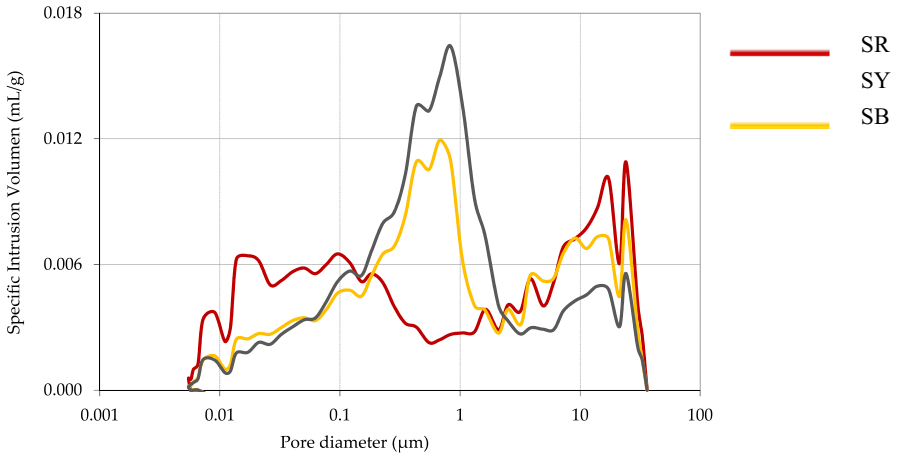

Fig. 6. Intrusion volume versus pore diameter determined through MIP.

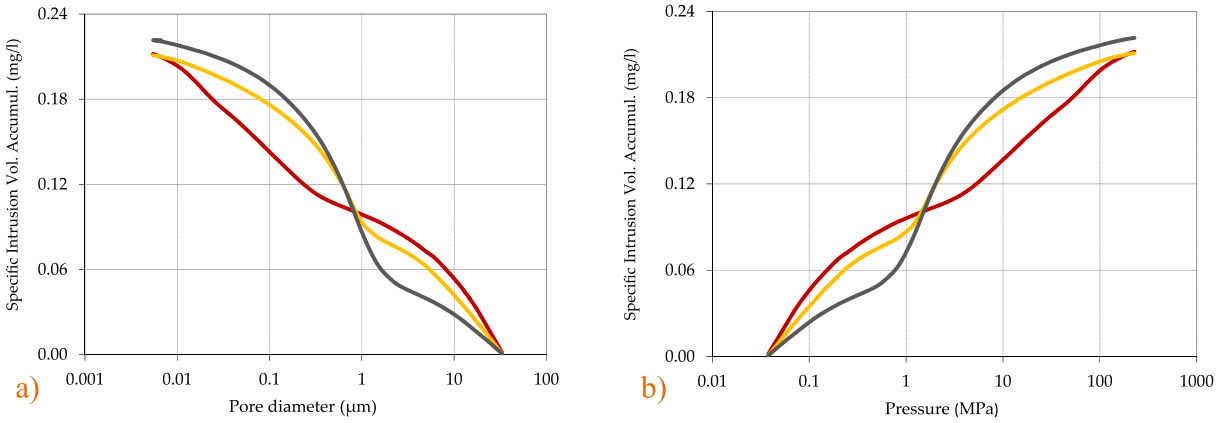

Fig. 7. a) Intrusion volume (accumulated) versus pore diameter determined through MIP and b) Intrusion volume (accumulated) versus pressure through MIP.

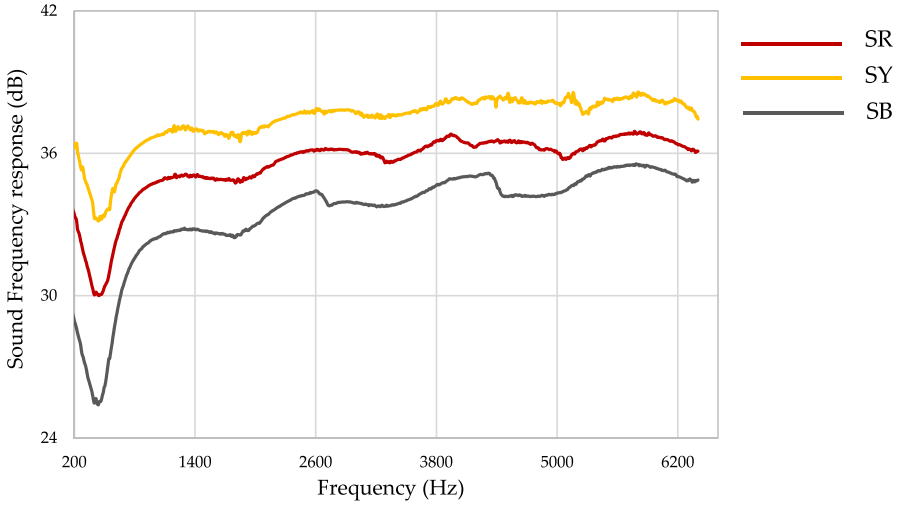

Fig. 8. Plotted sound frequency response results of the three soil-mixes, obtained as an average value from all the tested samples of each formulation.

ples. This data could be understood considering the mass law affecting the transmission of noise were, the greater mass the greater the insulation. This mass was quantified being, for SY samples, 19.5 kg/m^2, for SR samples, 19.3 kg/m^2, and, for SB sample, 16.5 kg/m^2.

Considering that the tube used covers a range of frequencies between 50 and 6400 Hz, it can be estimated that the resonant frequency of the samples is 440 Hz for SY samples, 448 Hz for SR samples, and 440 Hz for SB samples. In this case, SR samples present lower damping than the other two, implying a greater rigidity in this case.

An analysis of the results reveals the non-existence of resonances (presence or lack thereof of maxima and minima in an approximate range of 2 times the resonant frequency, meaning up to 1000 Hz) and the non-existence of critical frequencies in the range studied can also be established. However, the analysis has been carried out up to 6400 Hz, and they could be seen beyond this frequency. Although frequency response for building acoustics are only interesting from 100 to 3150 Hz in this paper the maximum range of results, depending on the tool sensitivity used, has been shown.

Another relevant aspect based on the acoustic analysis is that it did not show that the gradient of the curves increases by a 6 dB octave band, which implies a 6-dB increase in transmission losses when doubling the mass. This is due to the non-ceramic nature of the samples, made from raw soil stabilized through alginate polymer. Finally, from acoustic transmittance measurements, and considering the results, SY samples presented the greatest acoustic insulation properties.

Previous investigations reported a relationship between porosity and acoustic conductivity [67]. Moreover, it was found that an optimal pore in terms of aperture diameter ratio reduced average porosity and improved the sound absorption coefficient [68]. In the present investigation, it is not possible to establish such a direct correlation. An explanation for this could reside in the use of reinforcement fibers [69,70]; although all mixtures include fibers in the same proportion, the fiber–matrix interface may vary depending on the type of soil.

3.3. Thermal characterization

Results obtained by the thermal characterization of the tested samples provide a data range for the thermal conductivity coefficient between 0.53 and 0.68 W/mK. Specifically, these coefficients were determined to be 0.53 for SR, 0.68 for SY, and 0.61 for SB. In this test, the soil displaying the best thermal properties corresponded to the 'red' case, as shown by the results of the SR samples.

From a review of the literature, regarding the response to heat transmission of this type of material, it could be said that the results are within the obtained range, that is, between 0.5 and 1.0 W/mK, and even below the average of the most frequent thermal conductivity coefficients, i.e. between 0.7 and 1.0 W/mK [27,32,71,72].

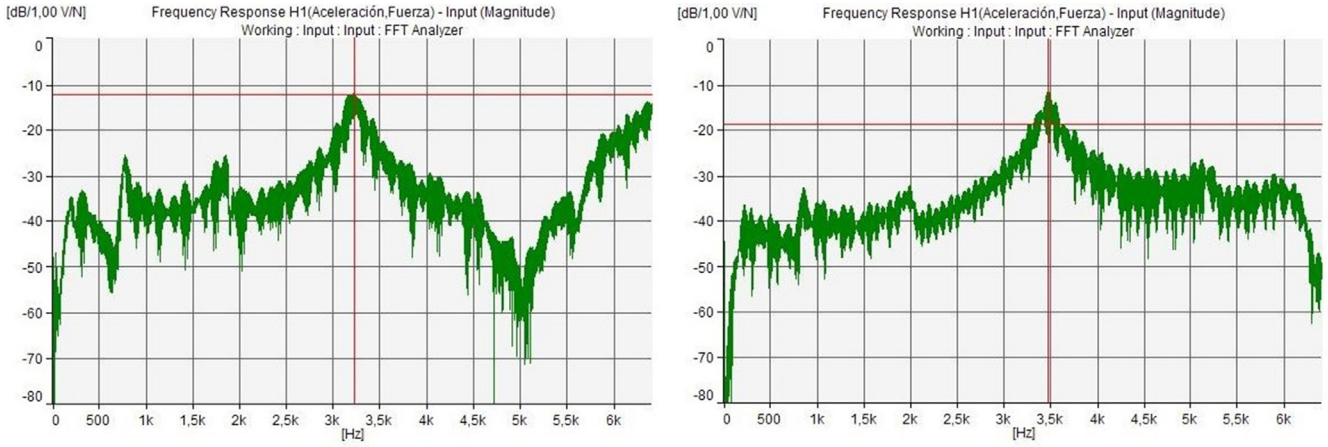

Fig. 9. Plotted impact graphs obtained during the MOE testing performance of two different samples of the SR formulation (amplitude error at the frequency peak 3500 Hz (dB) = -3.9224).

Table 4
Main results summary considering all the tests performed.

Test	Assessed value	Sample		
		SR	SY	SB
Density	Dry Bulk Density (kg/m^3)	1.510 (±90)	1.450 (±80)	1.390 (±130)
Thermal characterization	Thermal Conductivity (W/mK)	0,53	0,68	0,61
Acoustic characterization	Transmission Loss (dB)	X + 2	X + 4	X
	Resonant Frequency (Hz)	448	440	440
Youngs Modulus	Dynamic Modulus of Elasticity (GPa)	28,4	30,4	–
Mechanical testing	Compression strength (MPa)	3,85	3,79	1,70
	Flexural strength (MPa)	0,91	0,86	0,39
Internal Structure	Total Intrusion Volume (ml/g)	0,2120	0,2109	0,2216
	Total Pore Area (m^2/g)	14,681	7,322	6,825
	Diameter of Pore (Volume) (nm)	528,7	789,9	713,2
	Diameter of Pore (Area) (nm)	14,4	17,5	19,7
	Average Pore Diameter (nm)	57,8	115,2	129,9
	Bulk Density (A 0,0345 MPa) (g/ml)	1,7043	1,6986	1,4803
	Skeletal Density (g/ml)	2,6737	2,6496	2,2055
	Porosity (%)	36,18	35,85	32,83
Moisture	Moisture (W.B.) (%)	2,91	2,68	2,47
	Moisture (D.B.) (%)	3,00	2,75	2,53
Calorific (Heat) Capacity	High Calorific Value (D.B.) (Kcal/kg)	17,14	71,95	102,74
	Low Calorific Value (W.B.) (Kcal/kg)	16,64	70,02	100,20

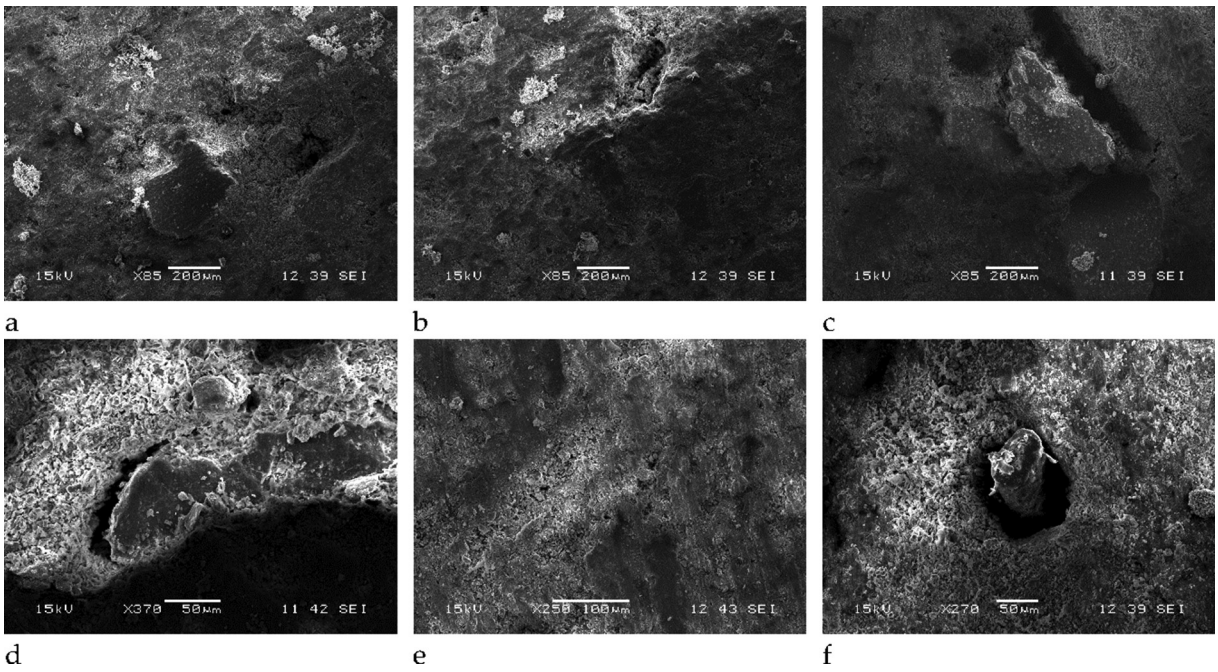

Fig. 10. a), b) and c) SEM images at low magnification SR, SY, SB respectively. And c), d) and f) SEM images at high magnification SR, SY, SB respectively.

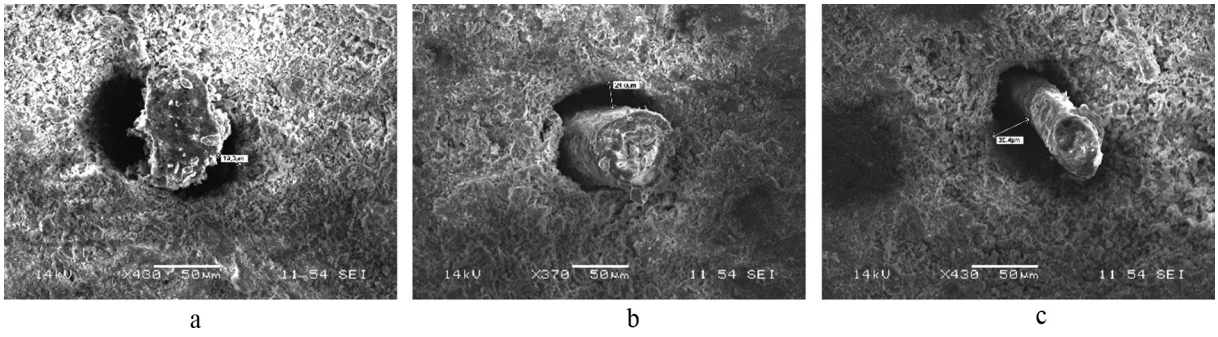

Fig. 11. Voids' radius measurements at the fiber–matrix interface for a) SR, b) SY, and c) SB.

In this case, it is also possible to establish a correlation between the results of thermal conductivity, dry bulk density, and total area of the pores tests [73,74]. This decrease in thermal conductivity could be associated with the decrease of dry bulk density and the increase of porosity. However, this correlation can be only established in the case of SR (with a dry bulk density of 1.510 kg/m3 and porosity of 36,18%) and SY (with a dry bulk density of 1.445 kg/m^3 and a porosity of 35,85%), unlike the case of SB (with a dry bulk density of 1.390 kg/m^3 and a porosity of 32,83%), since the dry bulk density decrease was mainly due to drying microcracks rather than a substantial porous network.

3.4. Dynamic Young's modulus (MOE)

The usual methods for the determination of the MOE are performed in the laboratory and are based on static tests allow an accurate measurement of stresses and deformations, or in the application of acoustic waves that easily determine the dynamic module. The latter, based on the application of acoustic waves generated from impacts, has been successfully used in other materials such as wood [75] concrete [76] and polymers [77].

For some specific materials, such as stone [78] and refractory products [79], there are standards for the determination of their MOE based on the application of analysis techniques of its resonance frequency. However, this standardization it is not specifically about mortars or stabilized earth materials, therefore, this research has followed the analysis methodology developed in this sense in previous works [80]. As an example, the results obtained for some of the test pieces of SR mix are shown below (Fig. 9).

The test could only be applied to two of the three formulations owing to the fact that the weak internal cohesion of the SB samples hampered the extraction of valid test results. These results corresponded to (28.0 ± 6.0) GPa for SR and (30.0 ± 7.0) GPa for SY, respectively. Although both parameters are similar, SY displays less mechanical stiffness than SR, which is consistent with the acoustic insulation properties of each of these mixes.

3.5. Results overview

The main results of the tests carried out on the three mixes analyzed in this work, SR, SY, and SB, are synthesized below. This

batch-format display aims to facilitate the cross-reading understanding of this data set (Table 4).

3.6. Additional performance considerations

Concerning the mechanical results, in the hardened state, a clear similarity can be appreciated in the performance at 28 days of SR and SY in both, the compression and flexural tests. Some relationships between porosity and mechanical performance can also be observed. Tests carried out with the SB formulation are in a strength range 40–60% lower compared to the previous ones. This difference cannot be fully explained by large disparities in dry bulk density or compactness of the samples. Rather, it must be interpreted in light of the plasticity test results that reveal higher degrees for both, plastic and liquid limit, for SB samples. These plasticity variations were verified in the specimens' manufacturing process and the subsequent curing defects.

The interpretation of the calorific value tests, both high and low, since the rest of the ingredients of the mixes are constant, must be done considering the components with the highest potential calorific value of each type of soil. In this sense, the chemical composition, richer in carbonates and possible organic compounds detected in the loss on ignition fraction of black and, to a lesser extent, yellow soils, would explain the remarkable increase in the values of SB and SY respectively. Apart from that, wet and dry basis moisture tests do not present noticeable dissimilarity in the values of the three mixes which would be consistent with porosity results in a correlated sequence of percentages.

In addition to MIP, the scanning electron microscopy (SEM) technique was also used in this research in order to determine the specificities of the porosity and microstructure of the samples. On the micrographic images, at low and high magnification, a series of porous networks and micro-cracks, due to the drying process and voids around the wool fibers, were observed (Fig. 10).

Further examination of the samples at the fiber–matrix interface implied variations in the radius measurements of these perimeter voids around the fibers. The difference may be due to the combination of the soil water retention curves owing to the different Atterberg limits of the soils (the highest index of plasticity 21.7% corresponds to SY, if compared to 11.5% for SR and 20.2% for SB) and the absorption–desorption processes of the wool fibers [81,82]. These measurements could be established in different ranges, being $\leq$ 20 μm for SR, between 20 and 30 μm for SY, and $\geq$ 30 μm for SB (Fig. 11). This data added to the average pore diameter extracted from the MIP tests, and considering that voids surround the fibers all along their length, could be translated into a certain heterogeneity in the size of the pores for a certain mixture favouring properties such as acoustic damping. In fact, the combination of these factors could properly explain the better acoustic performance of SY compared to SR and SB.

After the test benchmarking, for both, raw soils and hardened samples, it can be stated that: Atterberg limit is a key test to predict, for soils used as part of earthen materials stabilised with natural polymers and fibers, parameters related to dry bulk density and internal porous network characteristics. Furthermore, a direct correlation can be established between the samples dry bulk density results and mechanical performance. Regarding the thermal conductivity, total pore area and average pore diameter, are particularly significant sample features to be considered. While the acoustic performance, although also influenced by dry bulk density and porosity, results could be more affected by the homogeneity of the porous structure, so those factors that can alter it, such as fiber–matrix interaction during the curing process, must be observed.

4. Conclusions

This investigation analysed the effect of different soil types on the physical and mechanical characteristics of biocomposites made from soil stabilized with a natural polymer and reinforced with wool fibers. The work has identified parameters involved in their mechanical, thermal and acoustic performance to adapt these materials to the necessary technical and functional requirements. The design of the experimental programme, in addition to the characterisation of the soils themselves, was based on tests on hardened samples of three types of mixes with the only variable of the soil. The main conclusions of the study are summarized below:

The physical, chemical, and mineralogical characteristics of the soils, especially the different values of the Atterberg limits, modified mechanical, thermal, and acoustic properties of the mixtures. As expected, a direct relationship can be established between dry bulk density and porosity regarding mechanical performance results. The highest dry bulk density data, 1.510 (±90) kg/m^3 for SR, implies the highest mechanical results: 3,85 MPa (compression strength) and 0,91 MPa (flexural strength); similarly, the lowest density, 1.390 (±130) kg/m^3 for SB, implies the lowest mechanical results: 1,70 MPa (compression strength) and 0,39 MPa (flexural strength). However, this relationship was not linearly related in the case of all three soils due to the shrinkage and micro-cracks curing issues in SB samples. In addition to dry bulk density, average pore diameter and porosity are the samples features most affecting the thermal conductivity result. In this case the lowest conductivity, 0,53 W/mK for SR correspond with the highest dry bulk density data, 1.510 (±90) kg/m^3, the smaller average pore diameter 57,8 nm, and the highest porosity percentage, 36,18%. Porosity also affects dry bulk density and acoustic performance. Nevertheless, transmission loss is additionally affected by the use of reinforcement fibers and their impact in terms of open porosity.

These results prove that soil selection is a key factor in determining stabilized earth materials suitability. Their thermal performance and potential acoustic response are significantly dependent on appropriate soil selection. Consequently, the present research can serve as a basis for establishing the minimum criteria for both the selection of soils and the characterization of hardened samples.

Concerning future research arising from the results of this work, it would be interesting to analyze not only the soil effect, but the influence of adding different percentages and types of fibers to the mixes. On the other hand, considering moisture effects of these earthen materials, it seems appropriate for soil selection criteria, to establish a correlation between open porosity and capillary-water absorption and suction coefficients, with their impact on mechanical performance and thermal and acoustic insulation potential losses.

CRediT authorship contribution statement

Carlos Rivera-Gómez: Conceptualization, Methodology, Writing - original draft, Writing - review & editing. **Carmen Galán-Marín:** Supervision, Writing - review & editing. **Victoria P. López-Cabeza:** Funding acquisition. **Eduardo Diz-Mellado:** Funding acquisition.

Declaration of Competing Interest

The authors declare that they have no known competing financial interests or personal relationships that could have appeared to influence the work reported in this paper.

Acknowledgments

This work was supported by the TEP-1988 project PANEL of the call of the Dirección General de Investigación, Tecnología y Empresa. Consejería de Economía, Innovación, Ciencia y Empleo. Junta de Andalucía and the financial support of the Spanish Ministry of Education, Culture and Sport via two pre-doctoral contracts granted to Victoria López-Cabeza (FPU17/05036) and to Eduardo Diz-Mellado (FPU 18/04783). The authors wish to acknowledge the CITIUS, "Centro de Investigación, Tecnología e Innovación" of the University of Seville, X Ray Laboratory where the tests were carried out. We would also like to express our gratitude to the Foundation INNOVARCILLA, also known as the Andalusian Ceramics Technology Centre, for providing the different soils used within this research.

References

[1] N. Stern. Stern review on economics of climate change. Cambridge University Press; 2006. URL: http://journals.openedition.org/sapiens/240. ISBN: 978-2-8218-0808-9 ISSN: 1993-3819.
[2] IPCC, 2018: Global Warming of 1.5°C.An IPCC Special Report on the impacts of global warming of 1.5°C above pre-industrial levels and related global greenhouse gas emission pathways, in the context of strengthening the global response to the threat of climate change, sustainable development, and efforts to eradicate poverty [Masson-Delmotte, V., P. Zhai, H.-O. Pörtner, D. Roberts, J. Skea, P.R. Shukla, A. Pirani, W. Moufouma-Okia, C. Péan, R. Pidcock, S. Connors, J.B.R. Matthews, Y. Chen, X. Zhou, M.I. Gomis, E. Lonnoy, T. Maycock, M. Tignor, and T. Waterfield (eds.)]. In Press.
[3] United Nations – acting on climate change: the UN system delivering as one. DPI/2526; 2008.
[4] World Watch Institute – State of the World; 2009. ISBN: 978-0-393-33418-0.
[5] European Construction Sector Observatory - Analytical Report - Improving the human capital basis - April 2017. Available online: https://ec.europa.eu/docsroom/documents/24261 (accessed on 19 May 2020).
[6] CESCE. Informe sectorial de la Economía Española 2019. Available online: https://issuu.com/cesce.es/docs/informe_sectorial_cesce_2019 (accessed on 19 May 2020).
[7] H. Guillaud. Characterization of earthen materials. In: Avrami E, Guillaud H, Hardy M, editors. Terra literature review—an overview of research in earthen architecture conservation. Los Angeles (United States): The Getty Conservation Institute; 2008. p. 21–31. http://hdl.handle.net/10020/gci_pubs/terra_literature_review.
[8] H. Houben, P. Doat, L. Fontaine, R. Anger, W. Aedo, C. Olagnon, et al. Builders grains – a new pedagogical tool for earth architecture education. In: 5th International conference on building with earth – LEHM 2008, Weimar, Germany; 2008. p. 51–7.
[9] F. Pacheco-Torgal, S. Jalali, Earth construction: Lessons from the past for future eco-efficient construction, Constr. Build. Mater. 29 (2012) 512–519, https://doi.org/10.1016/j.conbuildmat.2011.10.054.
[10] UNE 41410:2008 Compressed earth blocks for walls and partitions. Definitions, specifications and test methods. AENOR. 2008.
[11] H. Schroeder, F. Volhard, U. Rohlen, C. Ziegert. The "Lehmbau Regeln" in 2008 – a review after 10 years of use in practice. In: 5th International conference on building with earth – LEHM 2008, Weimar, Germany; 2008. p. 13–21.
[12] HB 195 The Australian earth building handbook Dr Peter Walker MIEAust, CPEng. and Standards Australia. ISBN: 0 7337 4000 6. 2001.
[13] NZS 4297:1998 Engineering design of earth buildings... Available online: https://www.standards.govt.nz/sponsored-standards/building-standards/nzs4297/ (accessed on 19 May 2020).
[14] SADC ZW HS 983:2014: Rammed earth structures – Code of practice, is the national adoption of Southern African Development Community Cooperation in Standardization's (SADCSTAN) regional standard. Available online: http://www.rammedearthconsulting.com/library/african-rammed-earth-harmonised-standard-en.pdf (accessed on 19 May 2020).
[15] C.A. Dove, F.F. Bradley, S.V. Patwardhan, A material characterization and embodied energy study of novel clay-alginate composite aerogels, Energy Build. 184 (2019) 88–98, https://doi.org/10.1016/j.enbuild.2018.10.045.
[16] S. Sazedj, A. José Morais, S. Jalali, Comparison of environmental benchmarks of masonry and concrete structure based on a building model, Constr. Build. Mater. 141 (2017) 36–43, https://doi.org/10.1016/j.conbuildmat.2017.02.150.
[17] L. Assi, SeyedAli Ghahari, E. Deaver, D. Leaphart, P. Ziehl, Improvement of the early and final compressive strength of fly ash-based geopolymer concrete at ambient conditions, Constr. Build. Mater. 123 (2016) 806–813, https://doi.org/10.1016/j.conbuildmat.2016.07.069.
[18] A.H. Narayanaswamy, P. Walker, B.V. Venkatarama Reddy, A. Heath, D. Maskell, Mechanical and thermal properties, and comparative life-cycle impacts, of stabilised earth building products, Constr. Build. Mater. 243 (2020) 118096, https://doi.org/10.1016/j.conbuildmat.2020.118096.
[19] A.W. Bruno, D. Gallipoli, C. Perlot, H. Kallel, Thermal performance of fired and unfired earth bricks walls, J. Build. Eng. 28 (2020) 101017, https://doi.org/10.1016/j.jobe.2019.101017.
[20] Q. Li, R. You, C. Chen, X. Yang, A field investigation and comparative study of indoor environmental quality in heritage Chinese rural buildings with thick rammed earth wall, Energy Build. 62 (2013) 286–293, https://doi.org/10.1016/j.enbuild.2013.02.057.
[21] K.A.J. Ouedraogo, J.-E. Aubert, C. Tribout, G. Escadeillas, Is stabilization of earth bricks using low cement or lime contents relevant?, Constr. Build. Mater. 236 (2020) 117578, https://doi.org/10.1016/j.conbuildmat.2019.117578.
[22] E. Olacia, A.L. Pisello, V. Chiodo, S. Maisano, A. Frazzica, L.F. Cabeza, Sustainable adobe bricks with seagrass fibres. Mechanical and thermal properties characterization, Constr. Build. Mater. 239 (2020) 117669, https://doi.org/10.1016/j.conbuildmat.2019.117669.
[23] F. El Fgaier, Z. Lafhaj, E. Antczak, C. Chapiseau, Dynamic thermal performance of three types of unfired earth bricks, Appl. Therm. Eng. 93 (2016) 377–383, https://doi.org/10.1016/j.applthermaleng.2015.09.009.
[24] C.T.S. Beckett, R. Cardell-Oliver, D. Ciancio, C. Huebner, Measured and simulated thermal behaviour in rammed earth houses in a hot-arid climate, Part A: Struct. Behav. J. Build. Eng. 15 (2018) 243–251, https://doi.org/10.1016/j.jobe.2017.11.013.
[25] J. Tinsley, S. Pavía, Thermal performance and fitness of glacial till for rammed earth construction, J. Build. Eng. 24 (2019) 100727, https://doi.org/10.1016/j.jobe.2019.02.019.
[26] N. Jannat, A. Hussien, B. Abdullah, A. Cotgrave, Application of agro and non-agro waste materials for unfired earth blocks construction: A review, Constr. Build. Mater. 254 (2020) 119346, https://doi.org/10.1016/j.conbuildmat.2020.119346.
[27] P. Muñoz, V. Letelier, L. Muñoz, M.A. Bustamante, Adobe bricks reinforced with paper & pulp wastes improving thermal and mechanical properties, Constr. Build. Mater. 254 (2020), https://doi.org/10.1016/j.conbuildmat.2020.119314 119314.
[28] M. Saidi, A.S. Cherif, B. Zeghmati, E. Sediki, Stabilization effects on the thermal conductivity and sorption behavior of earth bricks, Constr. Build. Mater. 167 (2018) 566–577, https://doi.org/10.1016/j.conbuildmat.2018.02.063.
[29] L. Rincón, A. Carrobé, I. Martorell, M. Medrano, Improving thermal comfort of earthen dwellings in sub-Saharan Africa with passive design, J. Build. Eng. 24 (2019) 100732, https://doi.org/10.1016/j.jobe.2019.100732.
[30] P. Glé, E. Gourdon, L. Arnaud, Acoustical properties of materials made of vegetable particles with several scales of porosity, Appl. Acoust. 72 (5) (2011) 249–259, https://doi.org/10.1016/j.apacoust.2010.11.003.
[31] T. Gil-Lopez, M. Medina-Molina, A. Verdu-Vazquez, B. Martel-Rodriguez, Acoustic and economic analysis of the use of palm tree pruning waste in noise barriers to mitigate the environmental impact of motorways, Sci. Total Environ. 584-585 (2017) 1066–1076, https://doi.org/10.1016/j.scitotenv.2017.01.162.
[32] L. Randazzo, G. Montana, A. Hein, A. Castiglia, G. Rodonò, D.I. Donato, Moisture absorption, thermal conductivity and noise mitigation of clay based plasters: The influence of mineralogical and textural characteristics, Appl. Clay Sci. 132-133 (2016) 498–507, https://doi.org/10.1016/j.clay.2016.07.021.
[33] H. Binici, O. Aksogan, D. Bakbak, H. Kaplan, B. Isik, Sound insulation of fibre reinforced mud brick walls, Constr. Build. Mater. 23 (2) (2009) 1035–1041, https://doi.org/10.1016/j.conbuildmat.2008.05.008.
[34] M. Ben Mansour, E. Ogam, A. Jelidi, A.S. Cherif, S. Ben Jabrallah, Influence of compaction pressure on the mechanical and acoustic properties of compacted earth blocks: An inverse multi-parameter acoustic problem, Appl. Acoust. 125 (2017) 128–135, https://doi.org/10.1016/j.apacoust.2017.04.017.
[35] D.-R. Tămaş-Gavrea, T.-O. Dénes, Mechanical, thermal and acoustical properties of an innovative lime-wool composite, Procedia Manuf. 46 (2020) 402–409, https://doi.org/10.1016/j.promfg.2020.03.059.
[36] J. Niresh, S. Neelakrishnan, S. Subharani, R. Prabhakaran, Performance testing for sound absorption coefficient by using impedance tube, Res. J. Appl. Sci. Eng. Technol. 11 (2) (2015) 185–189, https://doi.org/10.19026/rjaset.11.1706.
[37] C. Galán-Marín, C. Rivera-Gómez, F. Bradley, The mechanical properties and molecular bonding characteristics of clay-based natural composites reinforced with animal fibres, J. Biobased Mat. Bioenergy 7 (1) (2013) 143–151, https://doi.org/10.1166/jbmb.2013.1269.
[38] E.K. Darling, C.J. Cros, P. Wargocki, J. Kolarik, G.C. Morrison, R.L. Corsi, Impacts of a clay plaster on indoor air quality assessed using chemical and sensory measurements, Build. Environ. 57 (2012) 370–376, https://doi.org/10.1016/j.buildenv.2012.06.004.
[39] Andalusian Ceramic Technology Center, INNOVARCILLA Foundation. 23710, Bailén, Jaén, Spain. http://www.innovarcilla.es/.
[40] ASTM D 422-63 (2007). Standard test method for particle-size analysis of soils. American Society for Testing and Materials, West Conshohocken, PA.
[41] ASTM D 4318–17 (2010). Standard Test Methods for Liquid Limit, Plastic Limit, and Plasticity Index of Soils, West Conshohocken, PA.
[42] CIMAPREM Food and Pharma Ingredients. 56130 Saint-Dolay – France. http://www.cimaprem.com/.
[43] C. Rivera-Gómez, C. Galán-Marín, F. Bradley, Analysis of the influence of the fiber type in polymer matrix/fiber bond using natural organic polymer stabilizer, Polymers (Basel) 6 (2014) 977–994, https://doi.org/10.3390/polym6040977.
[44] C. Galán-Marín, C. Rivera-Gómez, F. Bradley, Ultrasonic, molecular and mechanical testing diagnostics in natural fibre reinforced, polymer-stabilized

earth blocks, Int. J. Polym. Sci. 2013 (2013), https://doi.org/10.1155/2013/130582 130582.
[45] UNE-EN 772-13:2001. Methods of test for masonry units - Part 13: Determination of net and gross dry density of masonry units (except for natural stone).
[46] UNE-EN ISO 8894-1:2010. Refractory materials - Determination of thermal conductivity - Part 1: Hot-wire methods (cross-array and resistance thermometer) (ISO 8894-1:2010).
[47] UNE-EN 993-15:2005. Methods of test for dense shaped refractory products - Determination of thermal conductivity by the hot-wire (parallel) method.
[48] Polymethylmethacrylate (PMMA) Calibration Kit. Part Number :PL2020-0100 https://www.chem.agilent.com/store/productDetail.jsp?catalogId=PL2020-0100&catId=SubCat4ECS_32823.
[49] PULSETM analysis software. BRÜEL&KJAER. https://www.bksv.com/-/media/literature/Product-Data/bp1870.ashx (accessed on 19 May 2020).
[50] ASTM 1050-12. Standard Test Method for Impedance and Absorption of Acoustical Materials Using a Tube, Two Microphones and a Digital Frequency Analysis System. West Conshohocken, PA.
[51] ASTM E2611-17. Standard Test Method for for Normal Incidence Determination of Porous Material Acoustical Properties Based on the Transfer Matrix Method. West Conshohocken, PA.
[52] A.F. Soybert, Transfer function method for measuring characteristic impedance and propagation constant of porous materials, J. Acoust. Soc. Am. 86 (2) (1989), https://doi.org/10.1121/1.398241.
[53] D. Butkus, T. Januševicius, V. Aškelovic. Investigation of the variation of noise spectrum behind noise barriers made of different materials. 9th International Conference "ENVIRONMENTAL ENGINEERING" 22–23 May 2014, Vilnius, Lithuania. https://doi.org/10.3846/enviro.2014.007.
[54] S.S. Jung, Y.T. Kim. Y.B. Lee. Measurement of Sound Transmission Loss by Using Impedance Tubes. Journal of the Korean Physical Society, Vol. 53, No. 2, August 2008, pp. 596_600. https://doi.org/10.3938/jkps.53.596.
[55] ASTM E1875-13. Standard Test Method for Dynamic Young's Modulus, Shear Modulus, and Poisson's Ratio by Sonic Resonance. West Conshohocken, PA.
[56] P.A. Webb, C. Orr. Analytical Methods in Fine Particle Technology, Micromeritics Instrument Corp. Norcross, Georgia, USA, 1997. https://mail.micromeritics.com/Repository/Files/Modern_Methods_of_Particle_Characterization.pdf.
[57] P.A. Webb. An Introduction To The Physical Characterization of Materials by Mercury Intrusion Porosimetry with Emphasis On Reduction And Presentation of Experimental Data Micromeritics Instrument Corp. Norcross, Georgia, USA, 2001. https://www.micromeritics.com/pdf/app_articles/mercury_paper.pdf.
[58] ASTM D 4284-03. Standard Test Method for Determining Pore Volume Distribution of Catalysts by Mercury Intrusion Porosimetry. West Conshohocken, PA.
[59] ASTM D 4404-84 (reapproved 1992). Standard Test Method for Determination of Pore Volume and Pore Volume Distribution of Soil and Rock by Mercury Intrusion Porosimetry. West Conshohocken, PA.
[60] A. Hamraoui, T. Nylander, Analytical approach for the Lucas-Washburn equation, J. Colloid Interface Sci. 250 (2002) 415–421, https://doi.org/10.1006/jcis.2002.8288.
[61] UNE-EN 1015-11:2000/A1:2007. Methods of test for mortar for masonry - Part 11: Determination of flexural and compressive strength of hardened mortar.
[62] UNE-EN ISO 18134-1:2016: Solid biofuels. Determination of moisture content. Oven dry method. Part 1: Total moisture. Reference method.
[63] UNE-EN ISO 18134-2:2016: Solid biofuels. Determination of moisture content. Oven dry method. Part 2: Total moisture. Simplified method.
[64] UNE-EN ISO 18134-3:2016: Solid biofuels. Determination of moisture content. Oven dry method. Part 3. Moisture in general analysis sample.
[65] UNE-EN 14918:2011: Solid biofuels. Determination of calorific value.
[66] A.G. Mimboe, M.T. Abo, J.N.Y. Djobo, S. Tome, R.C. Kaze, J.G.N. Deutou, Lateritic soil based compressed earth bricks stabilized with phosphate binder, J. Build. Eng. 31 (2020), https://doi.org/10.1016/j.jobe.2020.101465 101465.
[67] H.K. Kim, H.K. Lee, Influence of cement flow and aggregate type on the mechanical and acoustic characteristics of porous concrete, Appl. Acoust. 71 (2010) 607–615, https://doi.org/10.1016/j.apacoust.2010.02.001.
[68] N. Neithalath, A. Marolf, J. Weiss, J. Olek, Modeling the influence of pore structure on the acoustic absorption of enhanced porosity concrete, J. Adv. Concr. Technol. 3 (2005) 29–40, https://doi.org/10.3151/jact.3.29.
[69] B. Rehder, K. Banh, N. Neithalath, Fracture behavior of pervious concretes: the effects of pore structure and fibers, Engin. Fracture Mechanics 118 (2014) 1–16, https://doi.org/10.1016/j.engfracmech.2014.01.015.
[70] I. Palomar, G. Barluenga, J. Puentes, Lime–cement mortars for coating with improved thermal and acoustic performance, Constr. Build. Mater. 75 (2015) 306–314, https://doi.org/10.1016/j.conbuildmat.2014.11.012.
[71] T. Santos, L. Nunes, P. Faria, Production of eco-efficient earth-based plasters: Influence of composition on physical performance and bio-susceptibility, J. Clean. Prod. 167 (2017) 55e67, https://doi.org/10.1016/j.jclepro.2017.08.131.
[72] S. Liuzzi, C. Rubino, P. Stefanizzi, Use of clay and olive puring waste for building materials with high hygrothermal performances, Energy Procedia 126 (2017) 234–241, https://doi.org/10.1016/j.egypro.2017.08.145.
[73] A. Laborel-Preneron, J.E. Aubert, C. Magniont, C. Tribout, A. Bertron, Plant aggregates and fibers in earth construction materials: a review, Const. Build. Mater. 111 (2016) 719e734, https://doi.org/10.1016/j.conbuildmat.2016.02.119.
[74] J. Lima, P. Faria. 2016. Eco-efficient earthen plasters: the influence of the addition of natural fibers. In: Fangueiro, R., Rana, S. (Eds.), Natural Fibres: Advances in Science and Technology towards Industrial Applications. RILEM Bookseries, vol. 12. Springer, Dordrecht, pp. 315e327. http://dx.doi.org/10.1007/978-94-017-7515-1_24.
[75] Fakopp: Acoustic tomography for tree evaluation, www.fakopp.com.
[76] A. Nagy, Determination of E-modulus of young concrete with nondestructive method, J. Mater. Civ. Eng. 9 (1) (1997) 15–20, https://doi.org/10.1061/(ASCE)0899-1561(1997)9:1(15).
[77] R. Schmidt, V. Wicher, R. Tilgner, Young's modulus of Goulding compounds mesured with a resonante method, Polym. Test. 24 (2005) 197–203, https://doi.org/10.1016/j.polymertesting.2004.08.010.
[78] UNE-EN 14146: Natural stone test methods - Determination of the dynamic modulus of elasticity (by measuring the fundamental resonance frequency) (2004).
[79] UNE-EN ISO 12680-1: Methods of test for refractory products - Part 1: Determination of dynamic Young's modulus (MOE) by impulse excitation of vibration (ISO 12680-1:2005) (2007).
[80] J.R. Rosell, I.R. Cantalapiedra. Simple method of dynamic Young's modulus determination in lime and cement mortars. Mater. Constr. Vol. 61, 301, 39-48, 2011 http://dx.doi.org/10.3989/mc.2010.53509.
[81] H. Zoriyeh, S. Erdem, E. Gürbüz, I. Bozbey, Nano-clay modified high plasticity soil as a building material: Micro-structure linked engineering properties and 3D digital crack analysis, J. Build. Eng. 27 (2020), https://doi.org/10.1016/j.jobe.2019.101005 101005.
[82] N. Huvaj, E. Uyeturk, Effects of drying on atterberg limits of pyroclastic soils of Northern Turkey, Appl. Clay Sci. 162 (2018) 46–56, https://doi.org/10.1016/j.clay.2018.05.020.